Effect of oxygen content on the transport properties of $LaTiO_{3+\beta/2}$ thin films

2006 J. Phys.: Condens. Matter 18 5835

(http://iopscience.iop.org/0953-8984/18/26/004)

INSTITUTE OF PHYSICS PUBLISHING JOURNAL OF PHYSICS: CONDENSED MATTER

J. Phys.: Condens. Matter **18** (2006) 5835–5847 doi:10.1088/0953-8984/18/26/004

Effect of oxygen content on the transport properties of $LaTiO_{3+\beta/2}$ thin films

F B Wang[1,2], J Li[1], P Wang[1,3], X H Zhu[1], M J Zhang[1], Z H Peng[1], S L Li[1], L P Yong[1,2], Y F Chen[1], X S Sun[2] and D N Zheng[1]

[1] Beijing National Laboratory for Condensed Matter Physics, Institute of Physics, Chinese Academy of Sciences, Beijing 100080, People's Republic of China
[2] Department of Materials Science, Sichuan University, Chengdu 610064, People's Republic of China
[3] Department of Physics, Yanbei Normal University, Datong, Shanxi 037000, People's Republic of China

E-mail: dzheng@ssc.iphy.ac.cn

Received 22 January 2006, in final form 6 May 2006
Published 16 June 2006
Online at stacks.iop.org/JPhysCM/18/5835

Abstract

The structural and transport properties of $LaTiO_{3+\beta/2}$ epitaxial thin films, grown at different oxygen pressures ranging from 6.6×10^{-4} to 5 Pa, have been investigated. X-ray diffraction peaks of the films shift to lower angles with increasing oxygen pressure, indicative of a variation of the corresponding lattice spacing. All the films show T^2 dependence of resistivity over a large temperature range of ~200 K, suggesting a band-filling-induced metallic Fermi-liquid behaviour. Upturns in resistivity have been revealed at low temperatures, which could be ascribed to the Anderson-localization effect caused by the cation vacancies. Furthermore, for the thin films grown at high oxygen pressures of 0.5 and 5 Pa, the dependence of resistivity on temperature shows a maximum at high temperatures. The maximum seems to support the argument that transition between t-orbital ordering and disordering plays an important role in dominating transport properties at high temperatures. Carrier density deduced from Hall coefficient increases with the decrease of oxygen content, and shows strong temperature dependence. From the experimental data, it can be asserted that in the $LaTiO_{3+\beta/2}$ thin films, besides the band filling effect, localization or disorder caused by La and Ti vacancy effects controls the unique transport properties.

1. Introduction

Strong electron–electron correlation has been attracting intensive interest motivated by the research of high temperature superconductivity. Many transition metal oxides with a partially occupied d-electron band are not conductors as expected by band theory, but indeed often

insulators [1]. It has been accepted widely that the insulating behaviour should be ascribed to the strong Coulomb repulsion among electrons, which opens a charge gap at the Fermi surface [2]. The filling-driven metal–insulator transition (MIT) is a striking property in the strong electron correlation systems, which is often accompanied by a tremendous series of unusual and complex phenomena, including high-temperature superconductivity, colossal magnetoresistance, and quantum phase transition [3–6]. Besides the MIT and the correlated insulator phase, the metal phase near the insulator is also intriguing, where fluctuations of spin, charge, and orbital correlation are dominant to some extent.

Recently, considerable renewed interest has been attracted in how the physical properties evolve with doping in the $LaTiO_3$ system. Stoichiometric $LaTiO_3$ is a Mott–Hubbard insulator with a G-type antiferromagnetic (AFM) ground state and a narrow charge gap of 0.2 eV, and shows orbital ordering due to the $GdFeO_3$-type distortion [3, 7]. Doping of these materials is done typically by substitution of a divalent cation of roughly the same radius as the trivalent La ion. $La_{1-x}Sr_xTiO_3$ is regarded as a candidate to investigate the influence of band filling on electronic properties since the end members $SrTiO_3$ and $LaTiO_3$ have d^0 and d^1 configuration, respectively. A possible electronic phase diagram [8] has shown that for a $La_{1-x}Sr_xTiO_3$ system, there are more likely two MITs. One occurs at a critical filling level $n_c(2)$ when holes are doped into the end compound $LaTiO_3$. The other one is at another critical filling $n_c(1)$ near the end compound $SrTiO_3$. On the insulating side of $n_c(1)$, an activated conductivity is expected, especially VRH (variable range hopping), if the disorder induced by the chemical doping is a sufficient perturbation. On the metallic side of $n_c(1)$, correlated metallic or Fermi-liquid behaviour is expected. The temperature dependence of resistivity, spin susceptibility and specific heat can all be interpreted by the Fermi liquid model [9]. When the system approaches $n_c(2)$ from the metal side, the conduction electron effective mass m^* is enhanced [10, 11], suggesting that the electron correlation becomes more and more significant here. By contrast, the situation near the MIT boundary at $n_c(2)$ is less clear. An alternative way to introduce carriers into the $LaTiO_3$ system is to increase its oxidation state by bringing about La or Ti vacancies, or inserting oxygen-rich layers into the lattice. The fully reduced phase $LaTiO_3$ is known as a Mott insulating Ti^{3+} compound, antiferromagnetic below $\sim$140 K [12]. The fully oxidized phase $LaTiO_{3.5}$ is ferroelectric [13] with a high ferroelectric transition temperature T_c (1500 °C). As the oxygen doping level is changed, the electronic properties evolve from a Mott insulator (Ti^{3+}) to a band insulator (Ti^{4+}), with a metallic region in between. An elegant work [14] has been done in La deficient $La_{1-x}Sr_xTiO_3$ samples ranging from antiferromagnetic insulating phase ($LaTiO_3$) to metallic phase ($La_{0.88}TiO_3$). In both the doping cases, the hole-doped level is enhanced for the systems derived from stoichiometric $LaTiO_3$. It has been corroborated that the strong electron correlation is weakened with increasing hole doping [8]. In contrast to $La_{1-x}Sr_xTiO_3$, the cation vacancies in the off-stoichiometric $LaTiO_{3+\beta/2}$ introduce a stronger perturbation to the periodic potential, which leads to a series of unique properties. Nevertheless, the $LaTiO_{3+\beta/2}$ system is much less investigated. There is rare evidence about how the metal–insulator transition evolves and how the correlation index U/W (U refers to the Coulomb interaction and W refers to effective d bandwidth) can be tuned while the oxygen doping is changed. The systematic scenario of the $LaTiO_{3+\beta/2}$ system about structural and transport properties has not been fully established.

At the same time, it should be noted that up to now the most attention has been focused on single crystals or polycrystals of these compounds, while the properties of thin films, especially $LaTiO_{3+\beta/2}$ thin films, have been rarely explored [15, 16]. The main challenge in investigating $LaTiO_{3+\beta/2}$ thin films systematically is to determine and to control the oxygen content effectively. In this paper, we tried to control the oxygen off-stoichiometry in $LaTiO_{3+\beta/2}$ thin films by varying the oxygen pressures during film deposition. The temperature dependence of

resistivity and structural properties of $LaTiO_{3+\beta/2}$ over a wide range of doping were studied. Hall measurements were carried out to determine the density and mobility of carriers. Besides the film crystallinity, much attention has been paid to clarify the main origin of the low-temperature resistivity minimum, the intermediate-temperature metallic behaviour and the high-temperature metal–insulator transition in $LaTiO_{3+\beta/2}$ films. After that, the resistivity was associated with Hall measurement in order to manifest the transport properties of $LaTiO_{3+\beta/2}$ thin films.

2. Experiment

The growth of $LaTiO_{3+\beta/2}$ epitaxial thin films was achieved by pulse laser deposition in a high-vacuum chamber using a polycrystalline target $LaTiO_{3.5}$. The target was fabricated by conventional solid-state reaction in flowing oxygen at 1370 °C for 10 h. A KrF excimer laser with 248 nm wavelength was used for ablation. The laser energy density was 2 J cm^{-2}. The temperature of the substrate, heated by a substrate heater block, was 750 °C, as measured by a pyrometer. The deposition time was 30 min with a laser repetition rate of 5 Hz. Single-crystal (001) $SrTiO_3$ substrates, which represent a small lattice mismatch between substrate and thin film, were used. The growth oxygen pressures were varied from 6.6×10^{-4} to 15 Pa for different samples. After growth the films were cooled down at a rate of 10 °C min^{-1} in the same oxygen pressure as in the growth process. At the beginning of decreasing temperature, a certain heating power should be kept in order to maintain the rate of 10 °C min^{-1}.When the heating power decreased to zero, the temperature was decreased to room temperature naturally. The crystal structure of these films was monitored *in situ* by reflection high-energy electron diffraction (RHEED), and *ex situ* by x-ray diffraction to determine the crystallographic orientation and lattice spacing. The electrical resistivity was measured with a four-probe method in the temperature range 5 K $< T <$ 300 K. In Hall measurement, Hall voltage (V_H) was monitored with the change of the magnetic field (B) up to ±5 T and the Hall coefficient was estimated from the V_H–B slope.

3. Structural properties

3.1. Crystal structure of films

By using x-ray diffraction, the orientation and crystallization of thin films were characterized. Figure 1 shows a θ–2θ scan along the $SrTiO_3$ (001) for $LaTiO_{3+\beta/2}$ thin films. Note that the diffraction peaks are very close to the substrate (00l) peaks. Taking into account that the $LaTiO_{3+\beta/2}$ system is derived from a perovskite-like layer structure [17], these diffraction peaks can be well indexed according to a pseudo-cubic lattice. The $(001)_C$ of thin films grown at 6.6×10^{-4} Pa appears at $2\theta = 22.44°$, then the resulting lattice parameter is 3.96 Å, almost equal to the lattice parameter of bulk $LaTiO_{3.0}$ (3.96 Å). The film diffraction peaks clearly shift to lower angles as the oxygen pressure is increased. The 5 Pa oxygen pressure leads to a diffraction peak at 21.3°, indicative of a larger lattice spacing, as compared with that for films grown at oxygen pressures 8×10^{-2} and 6.6×10^{-4} Pa. A higher oxygen pressure tends to increase the lattice spacing d. Ohtomo *et al* [15] previously have also observed a similar trend in their $La_{1-y}TiO_{3+\delta}$ thin films. The discrepancy among the diffraction angles can also be considered as an indication of the change of β with oxygen pressure in these films. Moreover, the interesting broadening, observed in diffraction peaks for the thin film fabricated at an oxygen pressure of 8.0×10^{-2} Pa, likely corresponds to a multiphase coexistence. We attempted to evaluate the Ti valence by x-ray photoelectron spectroscopy (XPS), then, to refine

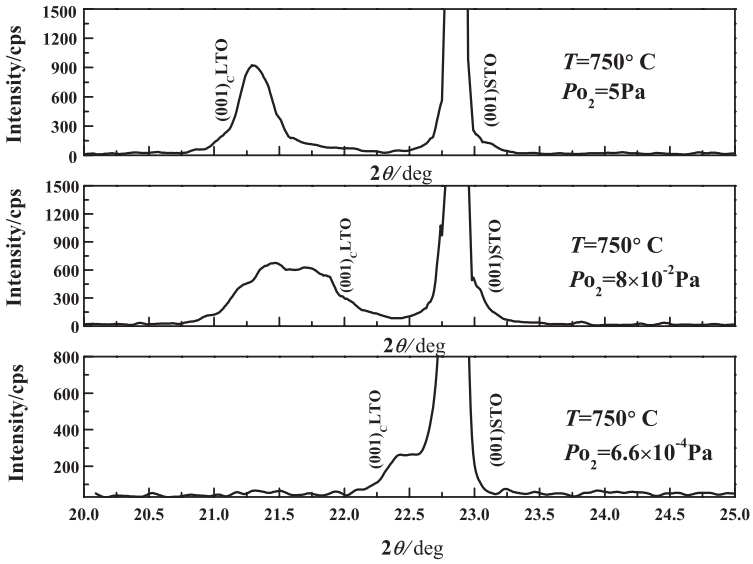

Figure 1. θ–2θ x-ray diffraction pattern of $LaTiO_{3+\beta/2}$ thin films deposited at (a) 5 Pa, (b) 8×10^{-2} Pa, and (c) 6.6×10^{-4} Pa.

the oxygen stoichiometry. This resulted in failure thanks to further oxidation of the film surface upon exposure to air [15].

3.2. In situ study of the film growth

In figure 2, typical RHEED patterns along the STO[110] azimuth are shown, yielding well defined streaks. The patterns were obtained in vacuum after film deposition. These streaks are located on Laue circles, indicative of smooth film surfaces and good in-plane orientations. The RHEED patterns also show some fine features indicating twin structures in the films.

4. Resistivity measurement

4.1. Intermediate-temperature metallic behaviour

In addition to structural properties, much attention has been paid to transport properties of $LaTiO_{3+\beta/2}$ thin films. We have measured the temperature dependence of resistivity for $LaTiO_{3+\beta/2}$ thin films grown at different oxygen pressures (P_o). As shown in figure 3, for samples deposited at $P_o = 5.0 \times 10^{-3}$, 8.0×10^{-3}, and 1.0×10^{-2} Pa, metallic behaviour is revealed and resistivity increases with temperature in a large temperature range over 200 K. Even for oxygen pressure 8.0×10^{-2} Pa, when the resistivity at room temperature reaches 4.3×10^{-3} Ω cm, metallic behaviour is still displayed from room temperature to ∼40 K. As well known, $LaTiO_3$ has been proved to be located in the immediate vicinity of the metal–insulator boundary. A low oxygen doping level of ∼0.03 would induce metallic behaviour, and the metallic region in the phase diagram of the $LaTiO_{3+\beta/2}$ system [17] expands until $\beta > 0.4$ (β refers to the nominal concentration of doped 'holes' per Ti site). Thereby, we have good reason to understand that metallic behaviour can exist in the film when P_o is as low as 5.0×10^{-3} Pa, and survive as long as a moderate P_o is applied. In the $LaTiO_{3+\beta/2}$ system, because there is no place to accommodate the interstitial oxygen in the TiO_6 octahedron, Greedan proposed

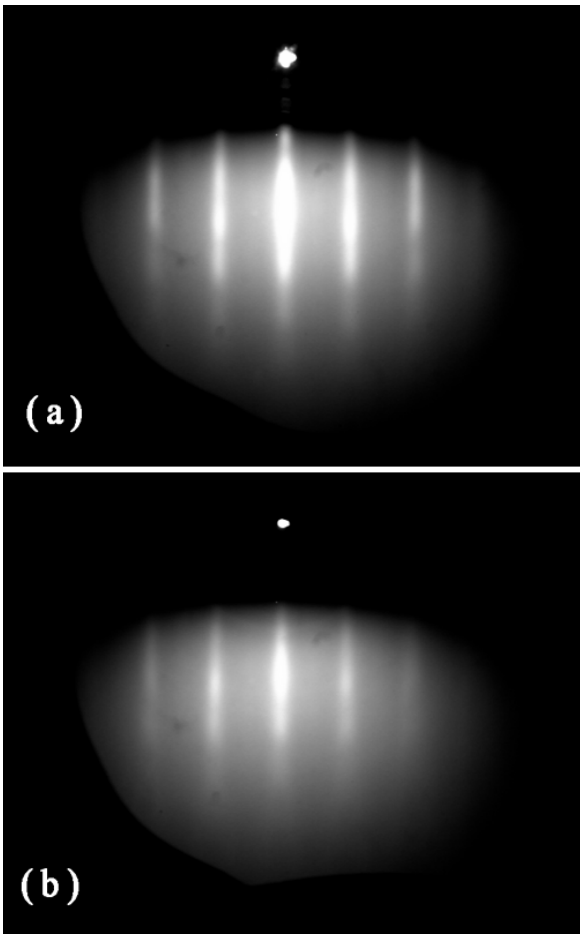

Figure 2. RHEED pattern observed after deposition along [110] azimuth for thin films grown at (a) 8.0×10^{-3} Pa, (b) 5.0×10^{-3} Pa.

that the $LaTiO_{3+\beta/2}$ should be designed as $La_{1-x}TiO_3$ [18, 14] and Goodenough believed that $LaTiO_{3+\beta/2}$ should be better represented by a formula of $La_{1-x}Ti_{1-y}O_3$ ($x > y$) [19, 20], that is to say, there is population of Ti vacancies besides La vacancies. The common point in the two formulas of $La_{1-x}TiO_3$ and $La_{1-x}Ti_{1-y}O_3$ is that the number of La vacancies is increased as a result of the increase in oxygen doping. A direct outcome followed by the increased La vacancies is the increase of Ti–O–Ti angle θ [18]. It was pointed out that the one-electron band width W, which is associated with θ, follows the form $W \propto \cos^2\theta$ [3]. Accordingly, it can be concluded that the band width W is increased with hole doping. The cubic/pseudocubic lattice parameter for the $SrTiO_3$ substrates used in this work is 3.905 Å. The pseudocubic perovskite lattice parameters of the $LaTiO_{3+\beta/2}$ thin films are larger than the standard lattice parameter 3.96 Å of $LaTiO_3$. Film epitaxy on $SrTiO_3$ therefore demands in-plane compressive strain of $LaTiO_{3+\beta/2}$ thin films. The compressive strain would decrease the in-plane Ti–O–Ti bond angle, resulting in the decrease of bandwidth W. The result contrasts with film epitaxy on $SrTiO_3$ of $NdNiO_3$ [21], and tensile strain straightens the in-plane Ni–O–Ni bond angle in a similar fashion to external hydrostatic pressure. In our work, all $LaTiO_{3+\beta/2}$ thin films

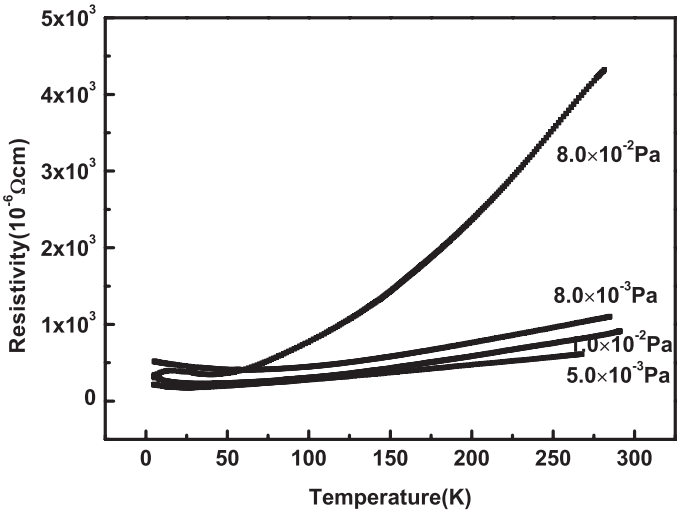

Figure 3. Temperature dependence of resistivity for samples deposited at different oxygen partial pressures.

were deposited on $SrTiO_3$ substrates. Thus we assume that the effects of compressive strain applied on the change of bandwidth W of $LaTiO_{3+\beta/2}$ thin films are similar. The variation of bandwidth W among different samples is mainly ascribed to the different oxygen content. When the band width W is increased with hole doping, the correlation index U/W is then decreased, as Coulomb repulsion U is approximately a constant [3], and the strong correlation is suppressed by oxygen doping. The decreasing U/W value eventually leads to the common existence of an itinerant-electron matrix (coherent state) [20], which likely corresponds to the dominant metallic electronic transport in $LaTiO_{3+\beta/2}$ thin films, different from that in the Mott–Hubbard insulator $LaTiO_3$ single crystal.

In figure 4 resistivity ρ for the selected samples was re-plotted versus T^2 to determine the metallic transport mechanism. Apparently the temperature dependence of resistivity can be fitted well by the $\rho = \rho_0 + AT^2$ relation, except the low-temperature deviations, which will be discussed in the next section. The T^2 dependence of resistivity was observed long ago in doped V_2O_3 [22]. This is indicative of a Fermi-liquid transport property, therefore likely corresponds to a mechanism that the electron–electron scattering rather than electron–phonon scattering dominates in the $LaTiO_{3+\beta/2}$ system. The induced T^2 dependence of resistivity by electron–electron correlation has also been conspicuously observed in Sr-substituted $Sr_{1-x}La_xTiO_3$ [9].

The apparent changes of transport properties in the films with different oxygen doping can be quantitatively evaluated by using the coefficient A of the T^2 term. The coefficient A gives the inelastic scattering strength between electrons. We plot A versus P_o in the inset of figure 4. For $P_o = 8.0\times10^{-2}$ Pa, the film shows the largest slope in the T^2 dependence of resistivity, and thus the largest coefficient A. While P_o decreases to 8.0×10^{-3} Pa, a considerable drop of coefficient A can be seen. $P_o = 5.0\times10^{-3}$ Pa induces an even smaller A. The slope abnormity in figure 4 for the film at $P_o = 1.0\times10^{-2}$ Pa is revealed to be just a slight fluctuation of A, as shown in the inset. It is clear that the coefficient A and thus the sample resistivity increase remarkably with the increasing oxygen doping in our $LaTiO_{3+\beta/2}$ thin films. It is accepted widely that oxygen doping results in a decrease in the band filling of Ti 3d electrons. The band filling n, which follows $n = 1-\beta$, reflects the number of 3d electrons per Ti site. Taking into account that A increases with oxygen doping, as indicated in the inset of figure 4, we can conclude that a lower

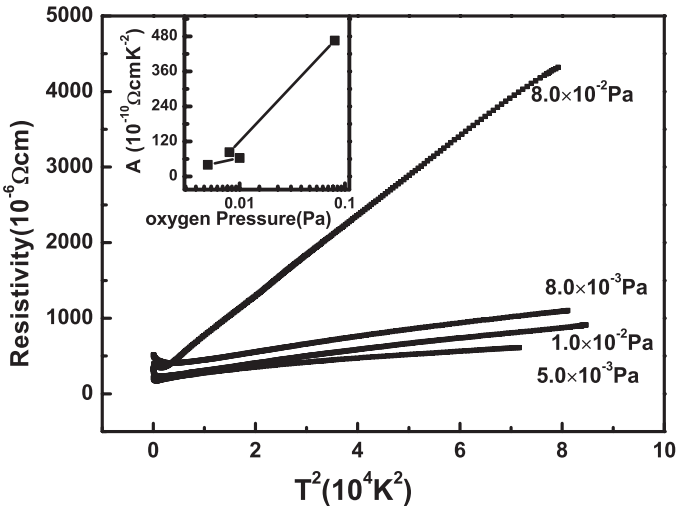

Figure 4. Temperature dependence of resistivity. ρ is plotted versus T^2. The inset shows a plot of the T^2 coefficient (A) of resistivity versus the oxygen pressure.

band filling n responds to a larger A. This does not agree with the conclusion that A increases with band filling n in $La_{1-x}Sr_xTiO_3$ [9]. Concerning the value of coefficient A, Greedan [18] inferred that a large A suggests a great level of correlation or localization. Because the strong correlation is suppressed by oxygen doping, just as stressed above, the large A, that is to say, is indicative of a large localization. The origin of this localization is more likely La or Ti vacancies.

4.2. Resistivity minima at low temperatures

Most of the films show an upturn at low temperatures, as demonstrated in figure 5. The upturn of resistivity at low temperatures can be observed for oxygen pressures from $P_o = 5.0 \times 10^{-3}$ to 0.5 Pa in our work, more ubiquitous than that reported by Taguchi *et al* [12] in single crystal $LaTiO_{3+\beta/2}$, where the resistivity minimum only exists as $\beta = 0.06$. We notice that the transition temperature for $P_o = 5.0 \times 10^{-3}$ Pa is 25.5 K, while for $P_o = 0.5$ Pa it amounts to 66.4 K. Such a minimum was found initially in structurally disordered metallic glasses like Co-rich metallic glasses [23] and amorphous alloys such as Cr–Pd–Si and Mn–Pd–Si alloys [24]. Kumar *et al* reported low-temperature resistivity minima in strongly correlated colossal magnetoresistive $La_{0.7}Ca_{0.3}MnO_3$ thin films [25]. Generally speaking, these works explained the resistivity minima in term of e–e interaction or Kondo effect. In the $LaTiO_{3+\beta/2}$ case, there are two electronic phases, strongly correlated electronic phase and itinerant electronic phase [20]. As pointed out by Goodenough [19, 20], increasing oxidation helps to reduce the electron–electron correlation, to decrease the band filling, and to induce high-density Ti vacancies in the $LaTiO_{3+\beta/2}$ thin films. The increasing Ti vacancies bring about a strong electronic potential perturbation, which, in turn, enhances the strong correlation fluctuation. A transition from strong-correlation electronic phase to itinerant electronic phase persists under strong correlation fluctuation. It was revealed that the cooperative dynamic itinerant electrons are in the Anderson-localized state as a result of strong potential perturbation [20]. With the transition from strong-correlation electronic phase to itinerant electronic phase, the Fermi surface level ε_F drops [26]. Before ε_F slides into the mobility edge, variable range hoping

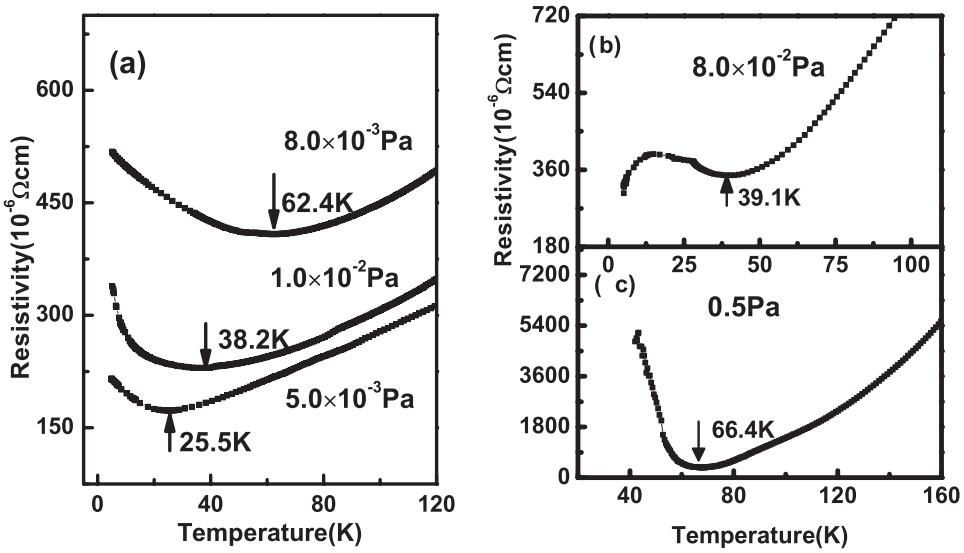

Figure 5. Low-temperature variation of resistivity for thin films deposited at oxygen pressure (a) 8.0×10^{-3} Pa, 5.0×10^{-3} Pa, and 1.0×10^{-2} Pa, (b) 8.0×10^{-2} Pa, and (c) 0.5 Pa.

transport behaviour associated with Anderson-localized states [19] appears, that is, the negative temperature derivative of resistivity. While ε_F falls below the mobility edge, the itinerant electron phase reaches a percolation threshold at a critical temperature, where the upturn of resistivity at low temperature appears [19].

4.3. High-temperature dependence of resistivity for thin films with high oxygen content

The resistivity versus temperature curve presents some interesting features at high temperatures for thin films deposited at oxygen pressures of 0.5 and 5 Pa, as demonstrated in figure 6. The latter shows a maximum at 258 K while a maximum is observed at 232 K for the former. The resistivity maxima are 5.4 Ω cm and 1.3×10^{-2} Ω cm, respectively. If we piece the low-temperature, intermediate-temperature, and high-temperature dependence of resistivity together for $P_o = 0.5$ Pa, a singular behaviour can be revealed, as shown in the inset of figure 6. Resistivity increases with decreasing temperature from high temperature to a maximum at 232.3 K followed by a decrease to a deep minimum at 66.4 K and another upturn appears at the lowest temperatures. The high-temperature resistivity decline has been predicted by Gariglio *et al* [16], based on a theory of small polaron conduction, and observed at 250 K in the $La_{1-x}Sr_xTiO_3$ system ($0.7 < x \leqslant 0.8$) by Hays [19], and at approximately 190 K for the $x = 0.8$ sample [16]. Here we prefer to interpret our experimental data according to orbital physics. Note that the resistivity maximum at high temperatures is only associated with samples grown at high oxygen pressures, 0.5 and 5 Pa, which correspond to a large concentration of La vacancies. It was pointed out that at a high oxidation level, the neighbouring La vacancies along the z-axis have different occupied probabilities. This discrepancy induces the trend that the Ti atom approaches the La site with lower occupied probability along the z axis. Therefore, a long Ti–O bond forms, connected with a short Ti–O bond. Due to the periodical structure of $LaTiO_{3+\beta/2}$, a structure order is obtained since every two long Ti–O bonds are connected with two short Ti–O bonds along the z axis [18]. The compression along the z axis associated with the short Ti–O bond allows the 3d electron to occupy the lower energy d_{xy} orbital. On the other

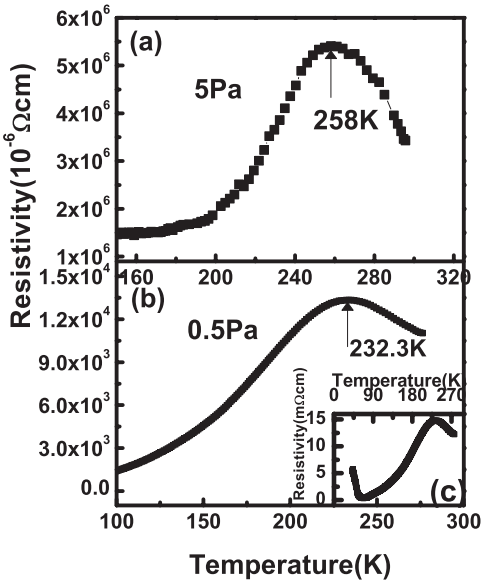

Figure 6. High-temperature dependence of resistivity for thin films grown at oxygen pressure (a) 5 Pa and (b) 0.5 Pa. The notations ↑, ↓ give the temperature at which metal–insulator transitions occur. Inset: the resistivity for 0.5 Pa thin film at a temperature range 5 K $< T <$ 275 K.

hand, the long Ti–O bands would cause the electron to occupy one of the higher energy d_{xz} and d_{yz} orbitals [27]. Accordingly, the structure order in Ti–O bond inevitably induces t-orbital order, and thus the high resistivity. With temperature increasing, the t-orbital order begins to collapse at a critical temperature, which causes the resistivity to begin dropping.

5. Hall measurement

To investigate the density and mobility of carriers in the films, we presented the results of Hall measurement. The sign of the Hall coefficient turned out to be negative for the three samples on which Hall measurements were carried out, indicating that electron-like charge carriers dominate electrical transport. According to a simple Drude model of $R_H = 1/ne$, where n refers to carrier density, and e refers to electron charge, carrier density with the variation of temperature is shown in figures 7–9. The plots suggest that carrier density shows strong temperature dependence for $P_o = 8 \times 10^{-2}$, 1.0×10^{-2} and 6.6×10^{-4} Pa. The R_H value is derived from the slope of transverse resistance as a function of magnetic field measured at different temperatures, shown in the inset of figures 7–9. The magnetic field from -5 to 5 T was applied to Hall measurement in a range of temperature from 5 to 250 K. For all three samples, the linearity of transverse resistance with magnetic field means that R_H is independent of magnetic field according to the formula $R_H = d\rho_{xy}/dH$. For $P_o = 1.0 \times 10^{-2}$ Pa (figure 7), the density of carriers increases with temperature; the estimated density of carriers is $n_H \approx 3.76 \times 10^{18}$ cm^{-3} at 25 K, and $n_H \approx 3.28 \times 10^{19}$ cm^{-3} of electrons at 250 K. When the temperature decreases below 25 K, a upturn in the variation of carrier density with temperature appears. The upturn, at 35 K, is more striking for the sample $P_o = 8 \times 10^{-2}$ Pa where n_H approaches approximately to 5.79×10^{18} cm^{-3} at 35 K, to 2.75×10^{19} cm^{-3} of electrons at 250 K (figure 8). At temperature higher than 35 K, the carrier density increases with temperature, which is consistent with the sample $P_o = 1.0 \times 10^{-2}$ Pa. Returning to the

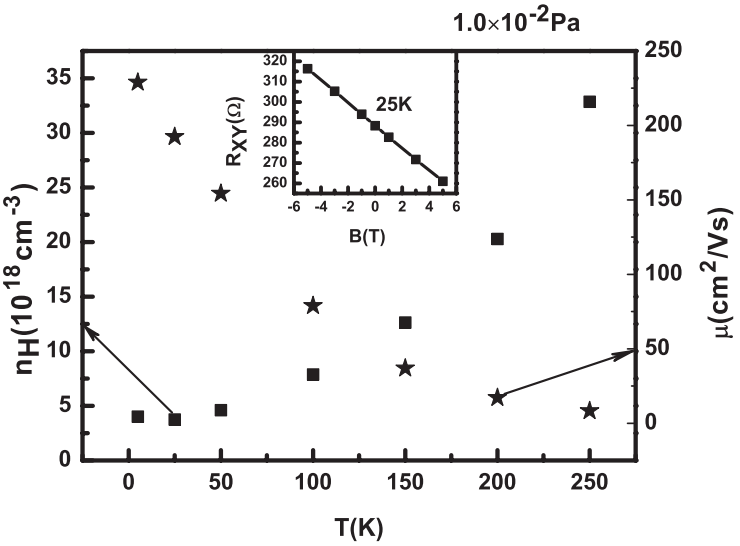

Figure 7. Carrier density and Hall mobility of sample $P_o = 1.0 \times 10^{-2}$ Pa. ■ and ★ show the carrier density and Hall mobility, respectively. Inset, transverse voltage as a function of magnetic field measured at 25 K.

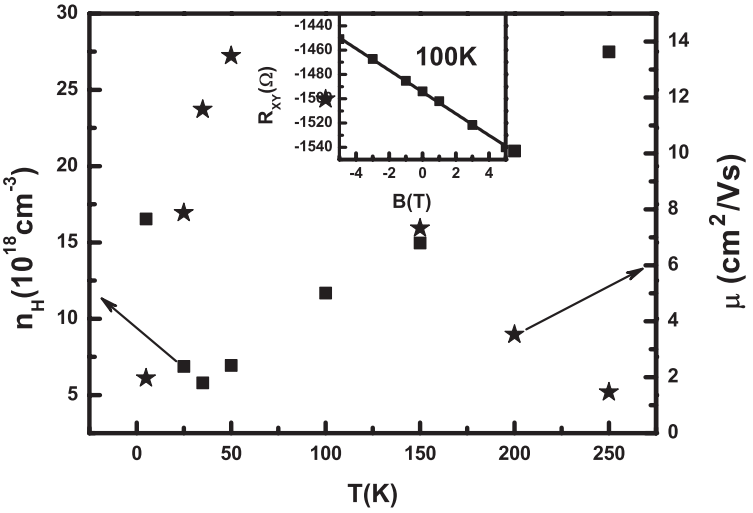

Figure 8. Carrier density and Hall mobility of sample $P_o = 8.0 \times 10^{-2}$ Pa. ■ and ★ show the carrier density and Hall mobility, respectively. Inset, transverse voltage as a function of magnetic field measured at 100 K.

resistivity variation with temperature for the three samples, it should be noted that the sample for $P_o = 6.6 \times 10^{-4}$ Pa is more metallic compared with the samples $P_o = 1.0 \times 10^{-2}$ Pa and $P_o = 8.0 \times 10^{-2}$ Pa. The more metallic characteristic, associated with high carrier density, was shown in the sample $P_o = 6.6 \times 10^{-4}$ Pa. The density of carriers is higher than those for $P_o = 1.0 \times 10^{-2}$ Pa and $P_o = 8.0 \times 10^{-2}$ Pa.

We focus firstly on the strong temperature dependence of carrier density, even for the sample $P_o = 6.6 \times 10^{-4}$ Pa where metallic transport is shown. However, the Hall coefficient

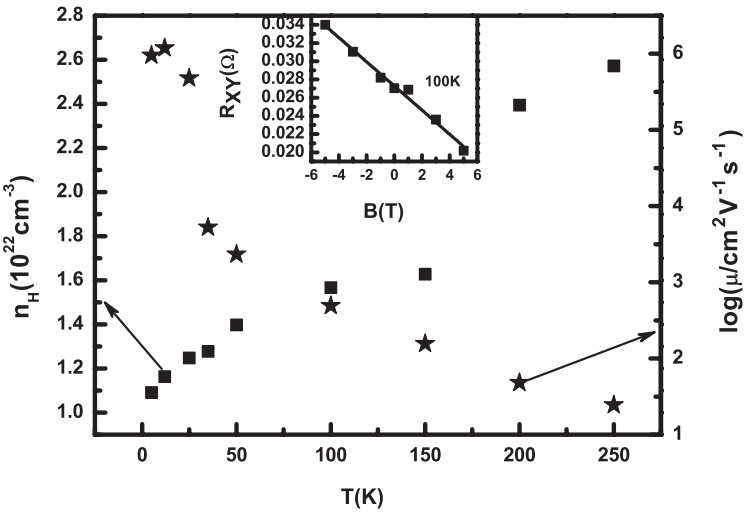

Figure 9. Carrier density and Hall mobility of sample $P_o = 6.6 \times 10^{-4}$ Pa. ■ and ★ show the carrier density and Hall mobility, respectively. Inset, transverse voltage as a function of magnetic field measured at 100 K.

in a metal is usually independent of temperature within the conventional Boltzmann transport framework. A temperature dependent Hall coefficient may arise from [28] (1) a narrow band (band width comparable to $\kappa_B T$), (2) a temperature dependent Hall factor (for a non-degenerate electron system), (3) two (or multi-) carrier conduction, or (4) magnetic skew scattering. The band width of $LaTiO_3$ W is 2.45 eV [29], which is much larger than $\kappa_B T$ at room temperature (0.0256 eV). In addition, magnetic skew scattering is associated with magnetic systems with spin–orbit coupling which do not include the $LaTiO_3$ system. Therefore, we exclude the possibility of narrow band and magnetic skew scattering to cause a temperature dependent Hall coefficient. However, much work is needed to determine whether a temperature dependent Hall factor or two (or multi-) carrier conduction dominates the temperature dependent Hall coefficient, because we have scarce evidence to specify the expression of Hall factor B as a function of temperature, and to testify the existence of two (or multi-) carriers. Takahashi *et al* [30] reported the temperature dependent Hall coefficient in Nb-doped $SrTiO_3$ thin films and he supported the argument that temperature dependent Hall coefficient is related to the existence of two types of carriers in doped $SrTiO_3$.

For $LaTiO_{3+\beta/2}$, a density of one carrier per Ti site gives the R_H value of 0.4×10^{-3} cm^3/C [12]. According to a simple Drude model of $R_H = 1/(ne)$, where n is carrier density and e is electron charge, we can deduce a conclusion that the maximum carrier density in the $LaTiO_{3+\beta/2}$ system is 1.56×10^{22} cm^{-3}. However, when we return to the variation of density carrier for sample $P_o = 6.6 \times 10^{-4}$ Pa, it is worth noting that at temperature higher than 150 K the density of carriers exceeds 1.56×10^{22} cm^{-3}. At 250 K, it approaches 2.57×10^{22} cm^{-3}. The same phenomenon has also been observed in Sr-doped $LaTiO_3$ thin films [31], and at the transition from p-type conduction to n-type conduction with the increase of Sr doping the carrier concentration drastically goes up to $n = 2 \times 10^{22}$ cm^{-3}, a density which is beyond the maximum density derived from the simple Drude model. Besides Sr doped $LaTiO_3$ thin films, the fact was also reported in an Sr doped $LaTiO_3$ single crystal [9]. The reason is not, to our knowledge, known.

According to the percolation model [32], the higher carrier density corresponds to more metallic transport, where the magnitude of Hall coefficient is dominated by carrier

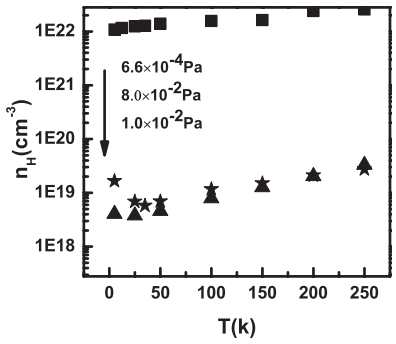

Figure 10. Carrier density as a function of temperature.

concentration in the metallic regions. Increasing oxygen content lowers carrier density. It is testified that when the carrier density is lower than the percolation threshold, activation over the barriers dominates, and there is a large contribution to the Hall effect from the barrier regions. Thereby, the sample $P_o = 6.6 \times 10^{-4}$ Pa shows higher density carrier than another two samples $P_o = 1.0 \times 10^{-2}$ and $P_o = 8.0 \times 10^{-2}$ Pa, as demonstrated in figure 10. The upturns in the variation of carrier density with temperature at 25 K for the sample $P_o = 1.0 \times 10^{-2}$ Pa, and at 35 K for the sample $P_o = 8.0 \times 10^{-2}$ Pa, can be interpreted by the tunnelling effect in the percolation model. When temperature is decreased below a critical temperature, tunnelling begins to make a significant contribution to conduction across barrier regions, and the Hall density begins to increase. It is at the critical temperature that the upturn occurs. The percolation model is established on the potential fluctuation caused by disorder, and the disorder causes the energy at the bottom of the conduction band to vary with position [33]. Thus, it strengthens the conclusion that disorder dominates the transport properties in $LaTiO_{3+\beta/2}$ thin films.

6. Concluding remarks

We have investigated the structural and transport properties of $LaTiO_{3+\beta/2}$ thin films grown at different oxygen pressures. X-ray diffraction patterns show that the diffraction peaks of thin films grown at higher oxygen pressures shift to lower diffraction angles. This suggests a variation of the lattice spacing and thus a change of the nominal hole doping in thin films. The temperature dependence of resistivity can be characterized by a given relationship $\rho = \rho_0 + AT^2$, indicative of a typical Fermi-liquid behaviour. The coefficient A increases with β, suggesting a strong vacancy-induced localization. At low temperatures, upturns in the temperature dependence of resistivity are exhibited. These upturns likely correspond to the Anderson-localization effect, the origin of which is considered to be cation vacancies as a result of oxygen doping. Interestingly, a maximum in high-temperature resistivity, for example a maximum resistivity at 258 K for thin films deposited at 5 Pa, was revealed in $LaTiO_{3+\beta/2}$ thin films. The maximum is probably associated with the transition between t-orbital ordering and disordering. It is the transition that dominates the transport properties at high temperatures for thin films with large oxygen doping. The Hall measurement showed that carrier density exhibits strong temperature dependence. It is interesting that with decreasing temperature we observed a upturn of carrier density in the samples $P_o = 8.0 \times 10^{-2}$ Pa and 1.0×10^{-2} Pa. This can be ascribed to the tunnelling at low temperature in the disordered $LaTiO_{3+\beta/2}$ system according to the percolation model. From the experimental data, the localization or disorder

induced by vacancies in band filling is considered to play a significant role in inducing these exceptional physical properties in $LaTiO_{3+\beta/2}$ thin films, different from that of divalent ion doped systems.

Acknowledgments

We are grateful to H Chen and S L Jia for measurements in structural and transport properties. A useful and stimulating discussion with J Y Xiang and P L Lang should be acknowledged. This work is supported by the National Natural Science Foundation of China under grant Nos 10574154, 50472076, and 10221002, the Ministry of Science and Technology of China, and the Chinese Academy of Sciences.

References

[1] de Boer J H and Verwey E J W 1937 *Proc. Phys. Soc.* **49** 59
[2] Mott N F and Peierls R 1937 *Proc. Phys. Soc.* **49** 72
[3] Masatoshi I, Atsushi F and Yoshinori T 1998 *Rev. Mod. Phys.* **70** 1039
[4] Sachdev S 2000 *Science* **288** 475
[5] Sokol A and Pines D 1993 *Phys. Rev. Lett.* **71** 2813
[6] Chakravarty S, Halperin B I and Nelson D R 1989 *Phys. Rev.* B **39** 2344
[7] Hemberger J *et al* 2003 *Phys. Rev. Lett.* B **91** 066403
[8] Amow G, Raju N P and Greedan J E 2000 *J. Solid State Chem.* **155** 177
[9] Tokura Y, Taguchi Y, Okada Y, Fujishima Y, Arima T, Kumagai K and Ige Y 1993 *Phys. Rev. Lett.* **70** 2126
[10] Georges A, Kotliar G, Krauth W and Rozenberg M J 1996 *Rev. Mod. Phys.* **68** 13
[11] Katsufuji T and Tokura Y 1994 *Phys. Rev.* B **50** 2704
[12] Taguchi Y, Okuda T, Ohashi M, Murayama C, Môri N, Iye Y and Tokura Y 1999 *Phys. Rev.* B **59** 7917
[13] Yamamoto J K and Bhalla A S 1991 *J. Appl. Phys.* **70** 4469
[14] Crandles D A, Timusk T, Garrett J D and Greedan J E 1994 *Phys. Rev.* B **49** 16207
[15] Ohtomo A, Muller D A, Grazul J L and Hwang H Y 2002 *Appl. Phys. Lett.* **80** 3922
[16] Gariglio S, Seo J W, Fompeyrine J, Locquet J-P and Triscone J-M 2001 *Phys. Rev.* B **63** 161103
[17] Lichtenberg F, Herrnberger A, Wiedenmamm K and Mannhart J 2001 *Prog. Solid State Chem.* **29** 1
[18] MacEachern M J, Dabkowska H, Garrett J D, Amow G, Gong W, Liu G and Greedan J E 1994 *Chem. Mater.* **6** 2092
[19] Hays C C, Zhou J-S, Markert J T and Goodenough J B 1999 *Phys. Rev.* B **60** 10367
[20] Zhou H D and Goodenough J B 2005 *Phys. Rev.* B **71** 165119
[21] Catalan C, Bowman R M and Gregg J M 2000 *J. Appl. Phys.* **87** 606
[22] McWhan D B, Menth A, Remeika J P, Brinkman W F and Rice T M 1973 *Phys. Rev.* B **7** 1920
[23] Majumdar A K, Khatua P K, Rathnayaka K D D and Nauqle D G 2004 *Phys. Rev.* B **69** 214417
[24] Hasegawa R and Tsuei C C 1970 *Phys. Rev.* B **2** 1631
[25] Kumar D, Sankar J, Narayan J, Singh R K and Majumdar A K 2002 *Phys. Rev.* B **65** 094407
[26] Zhou H D and Goodenough J B 2004 *Phys. Rev.* B **69** 245118
[27] Sunstrom J E, Kauzlarich S M and Klavins P 1992 *Chem. Mater.* **4** 346
[28] Ginsberg Donald M 1994 *Physical Properties of High Temperature Superconductors* (Singapore: World Scientific)
[29] Okimoto Y, Katsufuji T, Okada Y, Arima T and Tokura Y 1995 *Phys. Rev.* B **51** 9581
[30] Takahashi K S, Jaccard D, Triscone J-M, Shibuya K, Ohnishi T and Lippmaa M 2005 *Preprint* cond-mat/0508073
[31] Vilquin B, Kanki T, Yanagida T, Tanaka H and Kawai T 2005 *Appl. Surf. Sci.* **244** 494
[32] Juretschke H J, Landauer R and Swanson J A 1956 *J. Appl. Phys.* **27** 838
[33] Chien C L and Westgate C R 1980 *The Hall Effect and its Applications* (New York: Plenum)